Cellulose Nanofibrils from Sugarcane Bagasse as a Reinforcing Element in Polyvinyl Alcohol Composite Films for Food Packaging

Brian Victor Otenda, Patrick Gachoki Kareru, Edwin Shigwenya Madivoli, Ernest Gachui Maina, Sammy Indire Wanakai & Wycliffe Chisutia Wanyonyi

Published online: 06 Dec 2020.

Submit your article to this journal ☐

Article views: 135

View related articles ☐

View Crossmark data ☐

Taylor & Francis
Taylor & Francis Group

Check for updates

Cellulose Nanofibrils from Sugarcane Bagasse as a Reinforcing Element in Polyvinyl Alcohol Composite Films for Food Packaging

Brian Victor Otenda[a], Patrick Gachoki Kareru [iD][a], Edwin Shigwenya Madivoli [iD][a], Ernest Gachui Maina[a], Sammy Indire Wanakai[a], and Wycliffe Chisutia Wanyonyi[b]

[a]Chemistry Department, Jomo Kenyatta University of Agriculture and Technology, Nairobi, Kenya; [b]Department of Physical Sciences, University of Kabianga, Kericho, Kenya

ABSTRACT

Due to a high aspect ratio and enhanced mechanical strength, cellulose nanofibrils can be used as reinforcing elements in biocomposite films. In this study, cellulose nanofibrils were isolated from sugarcane bagasse using TEMPO-mediated oxidation and used to reinforce polyvinyl alcohol (PVA) films. The carboxyl group content, functional groups, crystallinity, thermal properties, and morphology of the nanofibrils were investigated. The influence of TOCNF content on the transmittance, swelling, and tensile strength of PVA-TOCNF films were investigated by varying the TOCNF content of PVA films. The fibrils had a carboxyl content of 12.2 ± 0.6 mg/g CE due to the presence of carboxylic groups, an increased degree of crystallinity, and highly porous nanofibrils with lengths between 150 nm and 600 nm. Incorporation of the isolated fiber on PVA films increased the swelling capacity, tensile strength, and UV absorption but a decrease in the solubility of the composite. An increase in the TOCNF content increased the tensile strength of the films with the highest tensile strength of 6.6 ± 2.2 kPa being observed when the TOCNF content was 30%. The improvement in films properties implies that the films can be used as a packaging material due to enhanced water absorption and light-barrier properties.

摘要
纤维素纳米纤维具有较高的长径比和较高的机械强度, 可作为生物复合材料薄膜的增强元件. 本研究利用TEMPO介导氧化法从甘蔗渣中分离出纤维素纳米纤维, 并用于增强聚乙烯醇（PVA）薄膜. 研究了纳米纤维的形态结构、功能基团、热性能. 通过改变聚乙烯醇薄膜中TOCNF的含量, 研究了TOCNF含量对PVA-TOCNF薄膜透过率、溶胀度和拉伸强度的影响. 由于羧基的存在、结晶度的增加以及长度在150-600nm之间的多孔纳米纤维, 纤维的羧基含量为12.2±0.6mg/gce. 在聚乙烯醇薄膜上掺入隔离纤维可提高复合材料的溶解度、拉伸强度和紫外吸收, 但降低了复合材料的溶解度. 随着TOCNF含量的增加, 薄膜的拉伸强度增加, 当TOCNF含量为30%时, 薄膜的拉伸强度最高为6.6±2.2kpa. 薄膜性能的改善意味着由于增强的吸水性和遮光性能, 薄膜可以用作包装材料.

Introduction

There is an enormous amount of lignocellulosic materials available from agricultural activities. Of these raw materials, at least 60 million tons of low-lignin cellulose fibers with different properties are produced annually by alkaline hydrolysis processes. The mechanical and chemical properties of these fibers highly depend on the raw materials used and the pulping conditions employed during isolation (Kekäläinen, Illikainen, and Niinimäki 2012). Cellulose is used commercially in textiles, the food

industry as a packaging material, paper making, textiles, drilling, chemical engineering, and architecture (Al-Hameedi et al. 2020; Du et al. 2017). A handful of investigations have been conducted to extract and utilize the cellulose nanofibrils (CNFs) from hydrolyzed residuals (Du et al. 2017). Cellulose nanofibers (CNF) are usually prepared using chemical, physical, biological, and oxidation methods (Kar, Rana, and Pandey 2015; Szczęsna-Antczak, Kazimierczak, and Antczak 2012). Chemical methods involve the use of strong acids where the amorphous domain of the fibers are destroyed yielding nanofibrils with esterified surface hydroxyl groups (Karimi and Taherzadeh 2016; Torres et al. 2013). When physical methods such as grinding at high speeds, high-intensity ultrasonic treatment, and mechanical nano fibrillation are employed, cellulose nanofibrils of nanometer diameter can be obtained (Boufi and Chaker 2016). Biological treatment involving enzymes such as cellulase is often coupled with mechanical/chemical methods to reduce the processing time and yield better CNF. This treatment also yields biocompatible cellulose nanofibrils that are environmentally friendly and are normally used to produce biomedical and pharmaceutical products such as wound dressings (Corgié, Smith, and Walker 2011; Szczęsna-Antczak, Kazimierczak, and Antczak 2012). CNF can also be obtained through oxidation using 2,2,6,6-tetramethylpiperidine-1-oxyl (TEMPO) as a catalyst which introduces a carboxyl group at the C_6 position yielding nanofibrils with a diameter of 3–4 nm (Isogai 2018; Jonasson et al. 2020; Menon et al. 2017). Due to their high aspect ratio and mechanical properties, the nanofibrils have been investigated as reinforcing elements in various polymetric matrixes as they improve the mechanical properties of the resulting composite material (Chowdhury et al. 2020; Kanai et al. 2020; Kar, Rana, and Pandey 2015). To improve the mechanical properties of PVA-based composites, both CNF and CNCs from various sources have been investigated as a reinforcing element. Bian et al. (2018) investigated the effect of loading CNF on the rheological and mechanical properties of PVA hydrogels. They observed that when 2% CNF was incorporated into the hydrogels, the storage modulus and young's modulus of the resultant hydrogels were increased 17-fold and 4-fold respectively (Bian et al. 2018). Miao et al. (2016) observed a remarkable increase in the storage modulus of up to 1090% higher when CNF was incorporated in the PVA matrix as compared to neat PVA films. In this study, the tensile strength of the resultant nanocomposite increased with a subsequent increase in the CNF content of the films with a tensile strength as high as 45 MPa being observed (Miao et al. 2016). In this study cellulose nanofibrils (CNFs) were isolated from sugarcane bagasse through TEMPO-mediated oxidation and used to enhance the tensile strength of polyvinyl alcohol films. Morphology of the fibers and the films was observed using a scanning electron microscope while fiber length distribution was determined using a transmission electron microscope. The crystallinity, carboxyl content, and functional groups present in the oxidized fibers and the films were also examined to determine the structural changes. The influence of TOCNF content on the transmittance, swelling, and tensile strength of PVA-TOCNF films were also investigated.

Materials and methods

Synthesis of cellulose nanofibrils

TEMPO-oxidized fibers (TOCNF) were synthesized according to the literature. In brief, 2 g of microcrystalline cellulose extracted from sugar cane bagasse were dispersed in 50 mL deionized water containing TEMPO (0.048 g) and sodium bromide (0.48 g). The oxidation was initiated by the addition of NaClO solution (30 mL) to the reaction vessel with continuous stirring while maintaining the pH at 10 by the addition of NaOH (0.5 M) solution during the reaction (Madivoli et al. 2020). The oxidation was carried out in an ultrasonicating bath at a frequency of 40 kHz and an output power of 150 W at a constant temperature of 50°C. After 3 h, the reaction was deemed complete when the pH of the solution remained constant at pH 10 without the addition of NaOH solution. The reaction was quenched by the addition of ethanol followed by washing to neutral pH and centrifugation several times to remove inorganics salts and TEMPO (Hassan and Hassan 2016; Jonasson et al.

2020; Rohaizu and Wanrosli 2017). Carboxylic content of the oxidized fibers was determined through titration in which one gram (1 g) of the sample was dispersed in 20 mL of double-distilled water for 1 h (Jiao et al. 2018; Rohaizu and Wanrosli 2017). To determine the degree of oxidation of the fibers, the samples were titrated against 0.1 M NaOH solution until pH 10 was monitored using a pH meter (Isogai 2018; Jonasson et al. 2020; Madivoli et al. 2020).

Determination of functional groups

The functional groups present in the reaction product were analyzed by a Bruker Tensor II FT-IR spectrophotometer model (Bruker, Ettlingen, Germany). The KBr pellets of samples were prepared by grinding 10 mg of samples, with 250 mg KBr (FT-IR grade). The 13 mm KBr pellets were prepared in a standard device under a pressure of 75 kN cm^{-2} for 3 min. The spectral resolution was set at 4 cm^{-1} and the scanning range from 400 to 4000 cm^{-1} (Madivoli et al. 2019, 2020; Ponce et al. 2013).

Powder X-ray diffractometer analysis

The crystallinity phase of the nanoparticles was identified using STOE STADIP P X-ray Powder Diffraction System (STOE & Cie GmbH, Darmstadt, Germany). The X-ray generator will be equipped with a copper tube operating at 40 kV and 40 mA and irradiating the sample with a monochromatic CuKα radiation with a wavelength of 0.1542 nm. XRD spectra was acquired at room temperature over the 2θ range of 5°–60° at 0.05° intervals with a measurement time of 1 s per 2θ intervals (Katata-Seru et al. 2018; Madivoli et al. 2019)

The XRD Crystallinity Index (CI_{XRD}) for native cellulose was calculated using the peak height method from the following height ratio:

$$CI(\%) = \left[\frac{I_{002} - I_{am}}{I_{002}} \right] x100 \qquad (2)$$

where I_{002} is the intensity of the 002 crystalline peaks at 22° and I_{am} the height of the minimum (I_{am}) between the 002 and the 001 peaks (Madivoli et al. 2019; Poletto, Heitor, and Zattera 2014)

SEM and TEM analysis

TEM analysis was performed on a Tecnai G2 Spirit (Thermo fischer scientific, Oregon USA) operated at 120kV equipped with veleta 2048 × 2048 wide-angle and Eagle 4096 × 4096 bottom mount detectors. The cellulose was suspended in ultrapure water (18MΩ.cm Barnstead Genpure UV-TOC, Thermo scientific, Germany) and ultrasonicated to obtain a solution of suspended fibers. The individual solutions were then drop casted in Carbon films 300 mesh (Electron microscopy science, CF300-CU) and dried to evaporate the solvent before TEM analysis (Jiao et al. 2018). The size of the nanofibrils were measured using the imaging processing software, ImageJ, and plotted as a histogram. Morphological analysis of dialdehyde cellulose were performed using Tescan Mira3 LM FE Scanning electron microscope operated at an accelerating voltage of 30 kV. The samples were gold-sputtered before observation to avoid the charging effect (Kia et al. 2017; Madivoli et al. 2019).

Thermal analysis

Thermal gravimetric analysis (TGA) and Differential Scanning Calorimetry (DSC) analysis were carried out using a Mettler Tolledo DSC/TGA 3+ (Mettler–Toledo GmbH, Switzerland). All the samples (10 mg) were heated from 25°C to 400°C, cooled to 25°C (Ciolacu, Ciolacu, and Popa 2011; Jonasson et al. 2020; Ponce et al. 2013)

PVA/cellulose composite films

The cellulose PVA nanocomposite films was prepared by dissolution and solvent casting the polymer matric in plastic molds as reported in the literature (Kanai et al. 2020). 1 g of PVA was dissolved in 50 mL distilled water at 60°C followed by the addition of TOCNF (0.1–0.5 g) to prepare solutions that had 10%–50% TOCNF. The solutions were vigorously stirred, ultrasonicated to remove air bubbles, poured in plastic molds, cured in an oven set at 50°C to constant weight, and stored in a desiccator before use (Kanai et al. 2020).

Thickness of the film

The thickness of the films was measured using a micrometer screw gauge to the nearest 0.001 mm. Measurements were made in at least seven random locations of each preconditioned film and the values were reported as mean ± standard deviation (SD). The mean values were used to determine the tensile strength of the dried films (Afonso et al. 2019; American Society for Testing and Materials 2018; Kanai et al. 2020; Zimet et al. 2019).

Water solubility

To determine the films solubility and swelling capacity, film pieces (20 × 20 mm) were dried at 105°C to constant weight followed by immersion in 50 mL of distilled water and shaken gently for 24 h at 25°C. The solutions were poured onto a filter paper (Whatman #1) to recover the undissolved films which were then weighed, and the wettability calculated using equation 1:

$$Swelling(\%) = \frac{Final\,wet\,weight - initial\,dry\,mass}{Initial\,dry\,mass} x100 \tag{1}$$

The film solubility was determined as the percentage of dry matter of the remaining film after immersion in water. Film pieces (20 × 20 mm) were dried at 105°C to constant weight followed by immersion in 50 mL of distilled water and shaken gently for 24 h at 25°C. The solutions were poured onto a filter paper (Whatman #1) to recover the undissolved films. The samples were then rinsed with distilled water and dried at 105°C to constant weight and the solubility was calculated according to equation 3 (Kanai et al. 2020; Zimet et al. 2019).

$$Solubility(\%) = \frac{Initial\,dry\,mass - final\,dry\,mass}{Initial\,dry\,mass} x100 \tag{2}$$

Tensile strength

The tensile strength was measured using an in house fabricated tensile strength device constructed from a laboratory ring stand to which a top horizontal support was attached (**Figure S1**). A weighing pan was used to hold the weights and reproducibility of the measurements were evaluated by measuring the tensile strength of a film with known strength using the same apparatus. The 5 × 1 cm film specimens were clamped in place and the total weight on the pan was increased by adding weights in a regular manner from 1 g to 500 g. The tensile strength was calculated by dividing the total load at the breaking point (in newtons) by the original cross-sectional area of the segment of the specimen that broke (in square meters) according to the following equation (American Society for Testing and Materials 2018; Stevens and Poliks 2003)

$$ts = \frac{W(kg).\left(9.80\frac{N}{kg}\right)}{A\left(10^{-4}\frac{m^2}{cm^2}\right)} \tag{3}$$

where W = total load, A = cross-sectional area of the film

Results and discussions

TEMPO oxidation of bagasse cellulose

The degree of oxidation of cellulose has been reported to be a function of reaction conditions and the type of biomass used during the production of cellulose nanofibers. For the case of reaction conditions, several authors have reported that the best reaction conditions to obtain the nanofibrils are room temperature and a reaction period of 16 h (Isogai 2018). The basic component for TEMPO-oxidized cellulose nanofibers are carboxylic acid functional groups introduced at the C-6 hydroxyl groups, which are sodiated at pH 10 (Madivoli et al. 2020). From this study, potentiometric titration of TOCNF against 0.1 M NaOH revealed that the carboxyl content of oxidized fibers to be 12.21 ± 0.6 mmol/g of fibers as compared to native-unoxidized cellulose that did not have carboxylic groups (Isogai 2018; Kanai et al. 2020; Zhou et al. 2018).

Determination of functional group present

The functional groups present in bagasse cellulose and TEMPO-oxidized cellulose (TOCNF) is depicted in Figure 1.

From Figure 1, the peaks between 3500 and 3300 are due to the surface hydroxyl groups while the peaks at 2900.3 cm^{-1} and 1328.9 cm^{-1} were attributed to CH_2 stretching vibrations of cellulose. The vibrational bands at 1213.1 cm^{-1} in the IR spectra were attributed to C-O stretching vibrations while the vibrational peak observed at 1070.4 and 850.5 cm^{-1} refers to the C-O-C vibrational frequency and β-glycosidic linkage vibration, respectively (Johar, Ahmad, and Dufresne 2012). The vibrational band observed at 1640 cm^{-1} corresponds to – OH bending vibrations as a result of cellulose water interaction (Jonoobi et al. 2010). As seen from the IR spectra of TOCNF, the fibers had all the vibration peaks associated with cellulose nanofiber except for the vibration peak at 1730 which is associated with C = O vibrational bands. TEMPO oxidation typical results in the oxidation of C6 carbon of cellulose resulting in the introduction of a carboxylic group at this position hence the observed carbonyl vibration peak (Jonasson et al. 2020; Jonoobi et al. 2010).
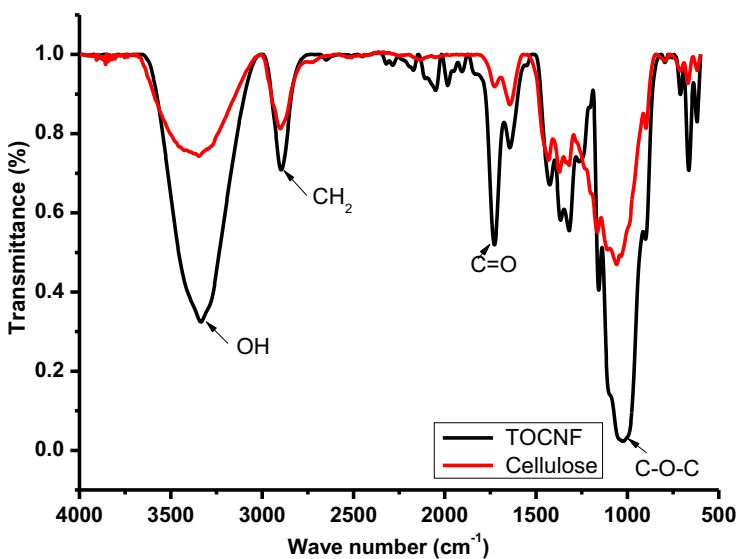

Figure 1. FT-IR spectra of native cellulose fibers and TOCNF.

Crystallinity changes

The X-ray diffractograms of TOCNF and SB-Cellulose are depicted in Figure 2.

Figure 2 shows the XRD patterns and corresponding crystallinity index (CrI) of cellulose bagasse after TEMPO oxidation. Cellulose is composed of both crystalline and amorphous domains which tend to influence the XRD diffractogram observed. The diffractogram of cellulose isolated from bagasse (Figure S1) was composed of crystalline cellulose domains which have peaks at 2θ angles of 16º, 22º, 34º, respectively, and were attributed to the diffraction planes of (101), (002) and (040) crystalline plane type 1 cellulose. The diffractogram of TOCNF had similar peaks at 2θ angles of 16º, 22º, 34º which is an indication that tempo oxidation does not result in changes in the crystallinity of the fibers. (Barbash, Yaschenko, and Shniruk 2017; Jonasson et al. 2020; Weng et al. 2017).

DSC thermogram of SB cellulose and SB TOCNF

The DSC thermograms of TOCNF isolated from sugarcane bagasse are depicted in Figure 3.

The DSC thermogram of cellulose was composed of an endothermic peak centered at 100°C associated with the evaporation of water on the surface of cellulose. A second endothermic peak associated with the decomposition of cellulose started at 298°C with maximum decomposition being observed at 338°C. The exothermic peaks occurring at 359°C and 482°C were attributed to the decomposition of hemicellulose and residual lignin present in cellulose samples after chemical treatment, respectively (Figure S2) (Jonasson et al. 2020). For the case of TOCNF, the first endothermic peak associated with water evaporation was centered at 44°C while the second endothermic peak associated with decomposition of cellulose was centered at 324°C. Differences in the thermal stability of cellulose during thermal decomposition was associated with changes in the size of the fibers as it has been reported that shorter fibers can easily dissipate heat hence the low thermal stability of TOCNF. Typically, the DSC thermogram of cellulose comprises of two endothermic peaks between 90°C and 120°C degrees and 320°C–360°C which are as a result of water evaporation and cellulose decomposition during analysis (Figure S2). The degradation of cellulosic components starts at 150°C and lasts up
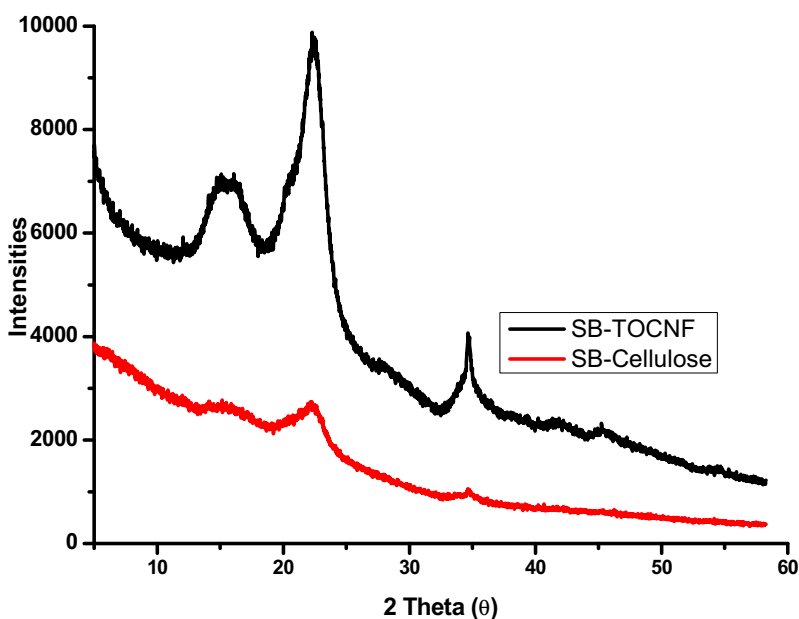

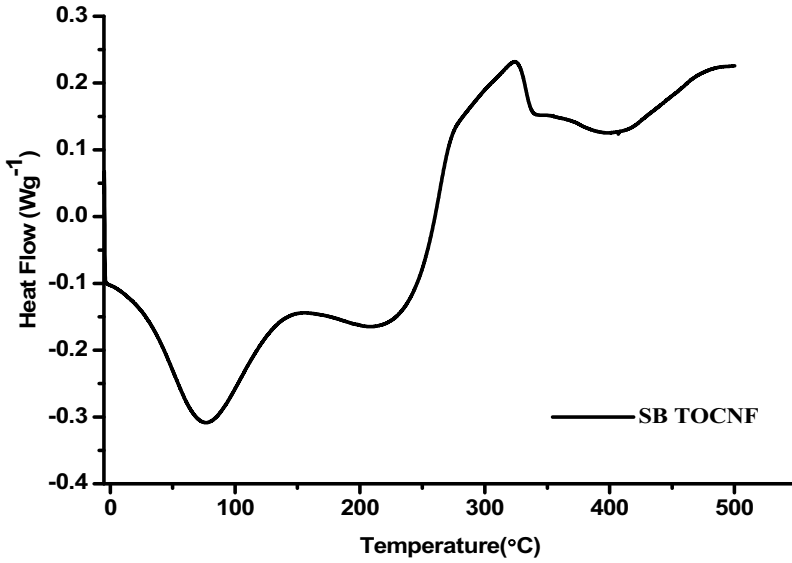Figure 2. X-ray diffractogram of TOCNF from sugar cane bagasse.

Figure 3. DSC thermogram of SB-cellulose fibers after TEMPO oxidation.

to 380°C when the decarboxylation, depolymerization, and decomposition occur in cellulose and hemicellulose fragments (Kian et al. 2017).

TGA thermograms of SB cellulose and SB TOCNF

The TGA-DTGA thermograms of cellulose nanofibrils isolated from bagasse are shown in Figure 4.

The first endothermic change occurs at 70°C–100°C due to evaporation of water and the second endothermic reaction which shows the degradation of hemicellulose structure, which is usually
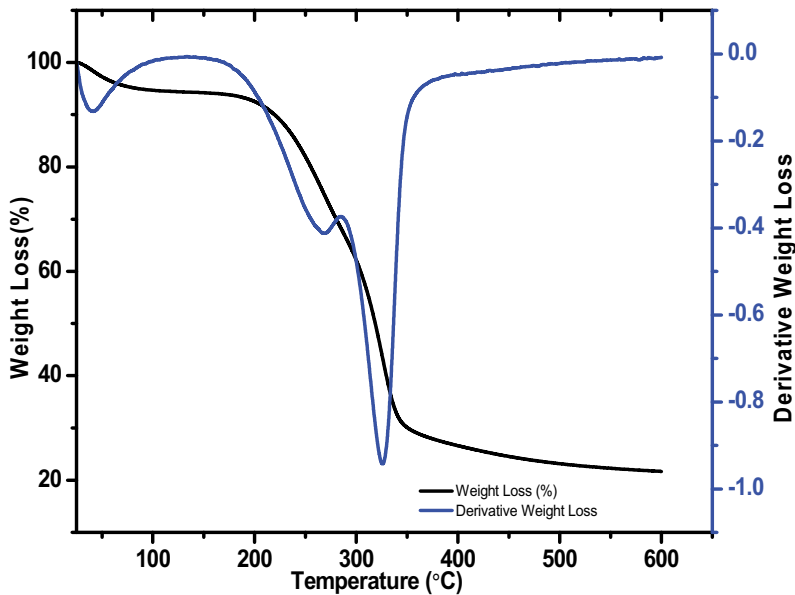

Figure 4. TGA/DTGA thermogram of SB-cellulose fibers after TEMPO oxidation.

observed between 180°C and 300°C. Generally, cellulose derived from natural fibers have high thermal stabilities due to α-cellulose of lignocellulosic structures. Similar results were observed in TGA thermograms in which all the samples underwent a small decomposition at around 150°C as a result of evaporation of bound water. All samples exhibited the cellulose decomposition process between 290°C and 360°C, which was ascribed to the removal of hemicellulose and lignin during the chemical pretreatment process (Jonasson et al. 2020; Madivoli et al. 2020).

Morphological analysis

The SEM micrographs depicting the morphology of the fibers after TEMPO oxidation is shown in Figure 5.

From Figure 5, chemical treatment of bagasse before TEMPO oxidation resulted into a yield of cellulose microfibrils composed of kinks and valleys as a result of lignin and hemicellulose removal during treatment. On the other hand, TEMPO oxidation of cellulose yielded a more porous, sponge-like fluffy mass containing sub-micrometer to micrometer wide long fibers which have been reported to be an indication of substantial self-assembly micrometer structures (Jiao et al. 2018). The network structure of the interconnected fibers made it difficult to measure the length of individual fibers observed during SEM analysis. The outstanding self-assembling behaviors of TEMPO-oxidized fibers may be ascribed to their much higher specific surface and hydrogen bonding capabilities as a result of their smaller dimensions and uniform structures during freeze-drying (Jiao et al. 2018).

TEM micrographs of SB TOCNF

The length distribution of TOCNF was evaluated using TEM and the micrographs obtained are depicted in Figure 6.

From Figure 6, it can be observed that the length of TOCNF from sugarcane bagasse was in the range between 150 nm and 600 nm. The length of cellulose nanofibrils obtained through TEMPO
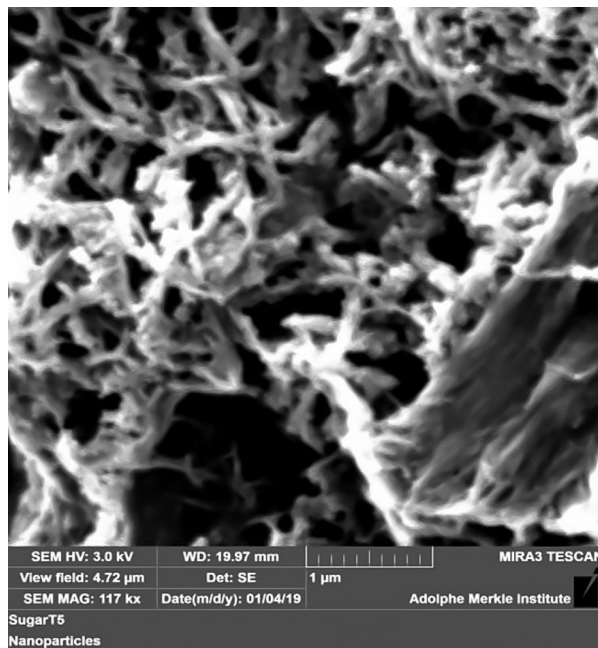

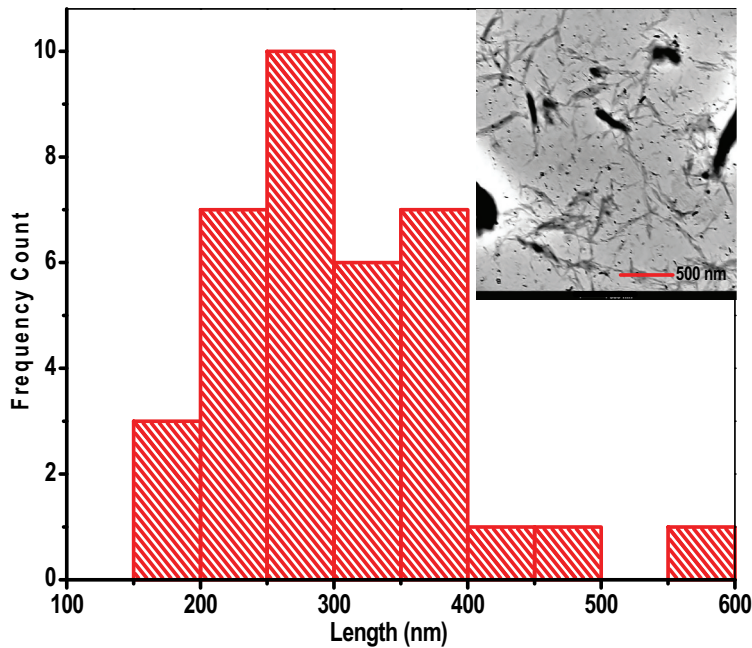
Figure 5. SEM image of SB TOCNF.

Figure 6. TEM micrographs and length distribution of SB-cellulose fibers after TEMPO oxidation.

oxidation is a function of the source of the fibers as different residues do give fibers with varying lengths. While this is so, the diameters of the fibers have been reported to be between 1 nm and 5 nm in length when the fibers are subjected to mild mechanical treatment after oxidation (Isogai 2018). Different authors have reported the synthesis of single strand fibers after oxidation and mild mechanical treatment, but in our study (Figure 6) the fibers obtained had widths similar to those reported in the literature but with no clear observable single fibers (Madivoli et al. 2020; Zhou et al. 2018).

Optical, swelling, mechanical properties of TOCNF-PVA films

The optical, swelling, mechanical properties of PVA films reinforced with TOCNF are depicted in Figure 7 and Table 1.

Films that are relatively transparent and bar ultraviolet radiation (UV) are generally considered to be of good quality (Cazón, Vázquez, and Velazquez 2018). UV light accelerates the oxidation of oils especially when influencers like chlorophyll are present (Mérillon and Gopal 2019). This in turn causes a change of taste and color, pruning down the nutritional value and shelf-life of the packaged food. Consumption of these kinds of foods poses harmful health effects that can be as grave as multiple sclerosis (MS) (Ahmed et al. 2016). Transparent packaging enables the consumer to undoubtedly tell the identity and quality of a packaged product before purchase (Jamshidian et al. 2012). The results show that the % Transmittance of the films reduced with each increase in the amount of blended cellulose as shown in Figure 7. The more the UV light was shielded the lesser the transparency of the films (Liu et al. 2013).

A major disadvantage of PVA-based films is their high solubility in water (Jain, Singh, and Chauhan 2017), making solubility tests an important parameter to check. To try and mend this defect, many studies have been directed toward crosslinking PVA-based films with other composites. The solubility of the films was determined after 24-h immersion in distilled water (50 mL) at room temperature (Silva et al. 2008). The percentage solubility was measured as the percentage dry mass of the solubilized film with respect to the total original mass of the film and the results are shown in
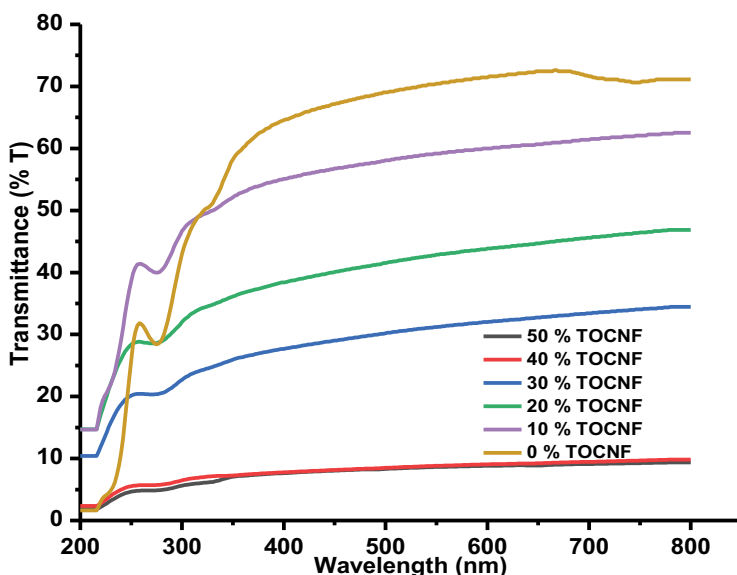
Figure 7. Optical transmittance of PVA films reinforced with Bagasse TOCNF.

Table 1. Swelling, thickness, solubility, transmittance (T_{600}), and tensile strength (t.s) of TOCNF-PVA films.

%CNF	Swelling (%)	Thickness (mm)	Solubility (%)	T_{600}%	t.s (kPa)
0	86.8 ± 3.4	0.302 ± 0.010	58.9 ± 0.8	71	1.1 ± 0.2
10	129.6 ± 3.4	0.160 ± 0.010	50.9 ± 1.4	60	1.2 ± 0.3
20	153.3 ± 6.6	0.214 ± 0.020	49.6 ± 4.1	44	5.4 ± 2.2
40	151.1 ± 3.4	0.246 ± 0.030	44.2 ± 1.4	32	5.6 ± 1.1
30	164.4 ± 3.4	0.338 ± 0.030	42.4 ± 0.8	9	6.6 ± 2.2
50	175.6 ± 3.4	0.384 ± 0.080	39.1 ± 2.0	9	3.4 ± 0.7

Table 1. Table 1 shows that the pure PVA film had a higher percentage of solubility whereas the solubility of the film decreased with an increase in the percentage TOCNF content in the blend film. The solubility of the PVA films prepared with blends of cellulose showed a decreasing trend as more cellulose was used. These results suggest that higher cellulose concentrations would be necessary to reduce the high solubility of pure PVA film. PVA is composed of – OH (hydroxyl groups) which have a high affinity for water molecules which raises their solubility of the resultant films. This also lowers its mechanical strength placing it at a relatively high disadvantage when it comes to its applications. The swelling behavior of the TOCNF-PVA composite blend films is shown in Table 1. The swelling characteristics of films are a very important parameter as it ties directly to their practical applications. For the composite films, it was noted that the swelling capacity was directly proportional to the amount of cellulose blended with the PVA as the higher the cellulose content the higher the swelling capacity. This slight increasing trend in the swelling capacity was attributed to water's great affinity for OH groups, which were presently availed by the nanocellulose fibers reinforcing the PVA films (Priya et al. 2014).

Conclusion

Cellulose nanofibrils were isolated from sugarcane bagasse using the kraft process followed by TEMPO-mediated oxidation. The oxidized fibers had high carboxyl content, which was visualized by slight changes in the degree of crystallinity, optical properties, carbonyl functional group, fiber morphology, and the length distribution of the fibers. Oxidation of the fibers resulted in yield loss of

cellulose that occurred during oxidation using TEMPO, which has been reported to cleave the crystalline domains in cellulose leading to shorter fiber lengths as visualized from TEM micrographs. Incorporation of the isolated fibers on PVA films increased the tensile strength, swelling capacity, and UV absorption of PVA films but it reduced the solubility of the resultant films in water.

Acknowledgments

Funding

ORCID

Patrick Gachoki Kareru 🆔 http://orcid.org/0000-0001-9622-6554
Edwin Shigwenya Madivoli 🆔 http://orcid.org/0000-0003-3992-5097

References

Afonso, C. R., R. S. Hirano, A. L. Gaspar, E. G. L. Chagas, R. A. Carvalho, F. V. Silva, G. R. Leonardi, P. S. Lopes, C. F. Silva, and C. M. P. Yoshida. 2019. Biodegradable antioxidant chitosan films useful as an anti-aging skin mask. *International Journal of Biological Macromolecules* 132:1262–73.

Ahmed, M., J. Pickova, T. Ahmad, M. Liaquat, A. Farid, and M. Jahangir. 2016. Oxidation of lipids in foods. *Sarhad Journal of Agriculture* 32:230–38.

Al-Hameedi, A. T. T., H. H. Alkinani, S. Dunn-Norman, M. A. Al-Alwani, A. F. Alshammari, M. M. Alkhamis, R. A. Mutar, and W. H. Al-Bazzaz. 2020. Experimental investigation of environmentally friendly drilling fluid additives (mandarin peels powder) to substitute the conventional chemicals used in water-based drilling fluid. *Journal of Petroleum Exploration and Production Technology* 10:407–17.

American Society for Testing and Materials. 2018. Standard test method for tensile properties of thin plastic sheeting, ASTM international. *ASTM D882-18, Standard Test Method for Tensile Properties of Thin Plastic Sheeting, ASTM International, West Conshohocken, PA*, www.astm.org

Barbash, V. A., O. V. Yaschenko, and O. M. Shniruk. 2017. Preparation and properties of nanocellulose from organosolv straw pulp. *Nanoscale Research Letters* 12:1–8.

Bian, H., L. Wei, C. Lin, Q. Ma, H. Dai, and J. Y. Zhu. 2018. Lignin-containing cellulose nanofibril-reinforced polyvinyl alcohol hydrogels. *ACS Sustainable Chemistry & Engineering* 6:4821–28.

Boufi, S., and A. Chaker. 2016. Easy production of cellulose nanofibrils from corn stalk by a conventional high speed blender. *Industrial Crops and Products* 93:39–47.

Cazón, P., M. Vázquez, and G. Velazquez. 2018. Cellulose-glycerol-polyvinyl alcohol composite films for food packaging: evaluation of water adsorption, mechanical properties, light-barrier properties and transparency. *Carbohydrate Polymers* 195:432–43.

Chowdhury, S., Y. L. Teoh, K. M. Ong, N. S. Rafflisman Zaidi, and S. K. Mah. 2020. Poly(Vinyl) alcohol crosslinked composite packaging film containing gold nanoparticles on shelf life extension of banana. *Food Packaging and Shelf Life* 24:100463.

Ciolacu, D., F. Ciolacu, and P. V. Popa. 2011. Amorphous cellulose—structure and characterization. *Cellulose Chemistry and Technology* 45:13–21.

Corgié, S. C., H. M. Smith, and L. P. Walker. 2011. Enzymatic transformations of cellulose assessed by quantitative high-throughput fourier transform infrared spectroscopy (QHT-FTIR). *Biotechnology and Bioengineering* 108:1509–20.

Du, L., J. Wang, Y. Zhang, C. Qi, M. Wolcott, and Z. Yu. 2017. Preparation and characterization of cellulose nanocrystals from the bio-ethanol residuals. *Nanomaterials* 7:51.

Hassan, E. A., and M. L. Hassan. 2016. Rice straw nanofibrillated cellulose films with antimicrobial properties via supramolecular route. *Industrial Crops and Products* 93:142–51.

Isogai, A. 2018. Development of completely dispersed cellulose nanofibers. *Proceedings of the Japan Academy Series B: Physical and Biological Sciences* Japan Academy.

Jain, N., V. K. Singh, and S. Chauhan. 2017. A review on mechanical and water absorption properties of polyvinyl alcohol based composites/films. *Journal of the Mechanical Behavior of Materials* 26:213–22.

Jamshidian, M., E. A. Tehrany, M. Imran, M. J. Akhtar, F. Cleymand, and S. Desobry. 2012. Structural, mechanical and barrier properties of active PLA-Antioxidant films. *Journal of Food Engineering* 110:380–89.

Jiao, L., H. Bian, Y. Gao, X. Lin, W. Zhu, and H. Dai. 2018. Highly dispersible cellulose nanofibrils produced via mechanical pretreatment and TEMPO-mediated oxidation. *Fibers and Polymers* 19:2237–44.

Johar, N., I. Ahmad, and A. Dufresne. 2012. Extraction, preparation and characterization of cellulose fibres and nanocrystals from rice husk. *Industrial Crops and Products* 37:93–99.

Jonasson, S., A. Bünder, T. Niittylä, and K. Oksman. 2020. Isolation and characterization of cellulose nanofibers from aspen wood using derivatizing and non-derivatizing pretreatments. *Cellulose* 27:185–203.

Jonoobi, M., J. Harun, A. P. Mathew, M. Z. B. Hussein, and K. Oksman. 2010. Preparation of cellulose nanofibers with hydrophobic surface characteristics. *Cellulose* 17:299–307.

Kanai, N., T. Honda, N. Yoshihara, T. Oyama, A. Naito, K. Ueda, and I. Kawamura. 2020. Structural characterization of cellulose nanofibers isolated from spent coffee grounds and their composite films with poly(Vinyl Alcohol): A new non-wood source. *Cellulose* 27:5017–28.

Kar, K. K., S. K. Rana, and J. K. Pandey. 2015. *Handbook of polymer nanocomposites.: processing, performance and application. volume B, carbon nanotube based polymer composites*. In *Volume* 195–211. B.Berlin: Springer Verlag.

Karimi, K., and M. J. Taherzadeh. 2016. A critical review on analysis in pretreatment of lignocelluloses: Degree of polymerization, adsorption/desorption, and accessibility. *Bioresource Technology* 203:348–56.

Katata-Seru, L., T. Moremedi, O. S. Aremu, and I. Bahadur. 2018. Green synthesis of iron nanoparticles using moringa oleifera extracts and their applications: Removal of nitrate from water and antibacterial activity against escherichia coli. *Journal of Molecular Liquids* 256:296–304.

Kekäläinen, K., M. Illikainen, and J. Niinimäki. 2012. Morphological changes in never-dried kraft fibers under mechanical shearing. *Cellulose* 19:879–89.

Kia, L., M. Jawaid, H. Ariffin, and O. Y. Alothman. 2017. Isolation and characterization of microcrystalline cellulose from roselle fibers. *International Journal of Biological Macromolecules* 103:931–40.

Kian, L. K., M. Jawaid, H. Ariffin, and O. Y. Alothman. 2017. Isolation and characterization of microcrystalline cellulose from roselle fibers. *International Journal of Biological Macromolecules* 103:931–40.

Liu, D., X. Sun, H. Tian, S. Maiti, and Z. Ma. 2013. Effects of cellulose nanofibrils on the structure and properties on PVA nanocomposites. *Cellulose* 20:2981–89.

Madivoli, E. S., P. G. Kareru, A. N. Gachanja, S. M. Mugo, and D. S. Makhanu. 2019. Synthesis and characterization of dialdehyde cellulose nanofibers from O. Sativa Husks. *SN Applied Sciences* 1:1–7.

Madivoli, E. S., P. G. Kareru, A. N. Gachanja, S. M. Mugo, D. M. Sujee, and K. M. Fromm. 2020. Isolation of cellulose nanofibers from Oryza Sativa Residues via TEMPO Mediated Oxidation. *Journal of Natural Fibers* 5:1–13.

Menon, M., R. Selvakumar, P. Kumar, and S. Ramakrishna. 2017. Extraction and modification of cellulose nanofibers derived from biomass for environmental application. *RSC Advances* 7:42750–73.

Mérillon, J.-M., and R. K. Gopal. 2019. *Bioactive molecules in food*. Food Chemistry. Cham, Switzerland.

Miao, X., F. Tian, J. Lin, H. Li, X. Li, F. Bian, and X. Zhang. 2016. Tuning the mechanical properties of cellulose nanofibrils reinforced polyvinyl alcohol composites: Via altering the cellulose polymorphs. *RSC Advances* 6:83356–65.

Poletto, M., O. J. Heitor, and A. J. Zattera. 2014. Native cellulose: Structure, characterization and thermal properties. *Materials* 7:6105–19.

Ponce, C., J. Chanona, V. Garibay, E. Palacios, G. Calderon, and R. Sabo. 2013. Functionalization of agave cellulose nanoparticles and its characterization by microscopy and spectroscopy techniques. *Microscopy and Microanalysis* 19:200–01.

Priya, B., V. K. Gupta, D. Pathania, and A. S. Singha. 2014. Synthesis, characterization and antibacterial activity of biodegradable Starch/PVA composite films reinforced with cellulosic fibre. *Carbohydrate Polymers* 109:171–79.

Rohaizu, R., and W. D. Wanrosli. 2017. Sono-assisted TEMPO oxidation of oil palm lignocellulosic biomass for isolation of nanocrystalline cellulose. *Ultrasonics Sonochemistry* 34:631–39.

Silva, G. G. D., P. J. A. Sobral, R. A. Carvalho, P. V. A. Bergo, O. Mendieta-Taboada, and A. M. Q. B. Habitante. 2008. Biodegradable films based on blends of gelatin and poly (Vinyl Alcohol): Effect of PVA type or concentration on some physical properties of films. *Journal of Polymers and the Environment* 16:276–85.

Stevens, E. S., and M. D. Poliks. 2003. Tensile strength measurements on biopolymer films. *Journal of Chemical Education* 80:810–12.

Szczęsna-Antczak, M., J. Kazimierczak, and T. Antczak. 2012. Nanotechnology-methods of manufacturing cellulose nanofibers. *Fibers & Textiles in Eastern Europe* 2:8–12.

Torres, F. G., O. P. Troncoso, C. Torres, and C. J. Grande. 2013. Cellulose based blends, composites and nanocomposites. *Advanced Structured Materials* 18:21–54.

Weng, R., L. Chen, S. Lin, H. Zhang, H. Wu, K. Liu, S. Cao, and L. Huang. 2017. Preparation and characterization of antibacterial cellulose/chitosan nanofiltration membranes. *Polymers* 9, 116:1–13.

Zhou, Y., T. Saito, L. Bergstrom, and A. Isogai. 2018. Acid-free preparation of cellulose nanocrystals by TEMPO oxidation and subsequent cavitation. *Biomacromolecules* 19:633–39.

Zimet, P., Á. W. Mombrú, D. Mombrú, A. Castro, J. P. Villanueva, H. Pardo, and C. Rufo. 2019. Physico-chemical and antilisterial properties of nisin-incorporated chitosan/carboxymethyl chitosan films. *Carbohydrate Polymers* 219:334–43.